**ORIGINAL ARTICLE**

# Design and Development of a Cold-Flow Test-Bench for Study of Advanced Nozzles in Subsonic Counter-Flows

Giuseppe Scarlatella[1] · Jan Sieder-Katzmann[1] · Florian Roßberg[1] · Felix Weber[2] · Carlos T. Mancera[1] · Daniele Bianchi[2] · Martin Tajmar[1] · Christian Bach[1]

## Abstract

As advanced nozzles may offer alternative solutions to conventional nozzles for the future class of reusable launch vehicles, a critical aspect is to tailor these novel technologies to current recovery strategies, more specifically to vertical landing sustained by retro-propulsion. Researchers at Technische Universität Dresden have developed a dedicated test-bench for the vacuum wind tunnel facility, where Advanced Nozzle Concepts (ANCs), such as aerospike and dual-bell nozzles, are tested in cold-gas configuration while invested by subsonic counter-flows. The main objective of the test campaign is to evaluate the performance and altitude–compensation characteristics of such ANCs by simulating a vertical landing manoeuvre through the variation of ambient pressure experienced during the landing burn. A detailed description of design and development of the test-bench, together with preliminary results from the commissioning activities, are here offered to the reader. The force measurements, together with pressure and temperature data, contribute to evaluate thrust levels and coefficients, as well as the monitoring of the interaction between the nozzle cold-flow and the opposing free-stream. A background-oriented schlieren system allows to visualise the external flow-field. In conclusion, an outline of the upcoming test campaign and a description of the expected results is offered.

✉ Giuseppe Scarlatella
   giuseppe.scarlatella@tu-dresden.de

   Jan Sieder-Katzmann
   jan.sieder-katzmann@tu-dresden.de

   Florian Roßberg
   florian.rossberg@mailbox.tu-dresden.de

   Felix Weber
   felix.weber@uniroma1.it

   Carlos T. Mancera
   carlos.tapia_mancera@tu-dresden.de

   Daniele Bianchi
   daniele.bianchi@uniroma1.it

   Martin Tajmar
   martin.tajmar@tu-dresden.de

   Christian Bach
   christian.bach1@tu-dresden.de

[1]  Institute of Aerospace Engineering, Chair of Space Systems, Technische Universität Dresden (TUD), Marschnerstr. 32, Dresden 01307, Saxony, Germany

[2]  Department of Mechanical and Aerospace Engineering, Università degli Studi di Roma "Sapienza", Via Eudossiana 18, Rome 00184, Lazio, Italy

## Abbreviations

| | |
|---|---|
| **AI** | Aerodynamics interference |
| **ALM** | Additive layer manufacturing |
| **ANC** | Advanced nozzle concepts |
| **AOA** | Angle-of-attack |
| **ASCenSIon** | Advancing space access capabilities–reusability and multiple satellite injection |
| **BOS** | Background-oriented schlieren |
| **CFD** | Computational fluid dynamics |
| **DAQ** | Data acquisition (system) |
| **DB** | Dual-bell (nozzle) |
| **ED** | Expansion–deflection (nozzle) |
| **NPR** | Nozzle pressure ratio |
| **RLV** | Reusable launch vehicle |
| **SLS** | Sea-level-standard |
| **SOTA** | State-of-the-art |
| **TUD** | Technische Universität Dresden |

# 1 Introduction

Recent achievements in the main stage recovery of the current class of Reusable Launch Vehicles (RLVs) [1–4] encourage the scientific community to question the effectiveness of bell nozzles by investigating critical phenomena that arise during a supersonic retro-propulsion phase [5, 6] and to push the State-Of-The-Art (SOTA) beyond the architectures adopted on the current generation of space transportation systems [7]. Advanced Nozzle Concepts (ANCs, see Figure 1) [8], such as aerospike, Dual-Bell (DB) and Expansion–Deflection (ED), may offer alternative solutions to the established bell nozzles thanks to their intrinsic altitude compensation capabilities. Differently from bell nozzles, which are optimized only for a specific altitude, these nozzle concepts achieve, in theory, a continuous (i.e., aerospike, ED) or stepwise (i.e., DB) adaptation to the atmosphere up to a designed nozzle pressure ratio [9]. This results in maximizing the nozzle efficiency at each altitude (below their designed height value) for continuously adapted nozzles, or at specific design points for stepwise adapted nozzles. The final outcome is an increase of the overall propulsive performance along the trajectory w.r.t. engines that adopt conventional bell nozzles and share a similar geometrical expansion ratio. Theoretically, this results in a payload gain (approximately from 5 to 20 % [10, 11], depending on configuration) or, alternatively, a more compact propulsive system. For this reason, ANCs are currently investigated in Europe across a wide spectrum. Recent research activities by Bolgar et al. [12, 13], within the collaborative research cluster Transregio 40, tested DB nozzles with supersonic and transonic external-flows, to simulate ascend phases and to trigger controlled transitions between the operative modes. Different projects under development within Technische Universität Dresden (TUD) [14–18] involve aerospike engines/nozzles in both cold-flow and hot-gas configurations. Furthermore, private companies start dedicating part of their resources to investigate aerospike engines as solutions for propulsion systems on main stages [10]. Moreover, ED nozzles are currently investigated by "Sapienza" University of Rome

as they may constitute a valid alternative for upper stages thanks to their high expansion-ratios for a reduced volume w.r.t equivalent bell nozzles. Despite this, they are generally not considered an effective alternative for main stages (with the exception of some single-stage-to-orbit case studies [11, 19]).

To validate their applicability within future generations of RLVs, it comes as a necessity to test ANCs in retro-propulsion and unpowered (engine-off) counter-flow scenarios. A typical re-entry path for a reusable main stage at the current SOTA (recovery strategy based on powered vertical-landing manoeuvres) faces at least three distinct phases [1, 5]: re-entry burn (from low-hypersonic to low-supersonic counter-flows), aerodynamic re-entry at engine-off (mostly supersonic) and landing burn (from supersonic to low-subsonic). The main focus of the current test campaign at TUD is to simulate in a vacuum wind tunnel the low-subsonic phases of a landing burn manoeuvre. The test-bench developed for this scope and hereby introduced is equipped with advanced nozzles specimens that allow comparative studies with conventional nozzles and investigations on the effects of retro-propulsion on their altitude–compensation properties. In addition, ANCs tested at design point in near-vacuum conditions are case of interest too. This double application of the test-bench allows to simulate ANCs in variable ambient-pressure conditions, from near-vacuum ($\sim 7\,kPa$) to Sea Level Standard (SLS).

The article presents a detailed description of the methodology adopted in Sect. 2, leaving additional details on altitude–compensation mechanisms to references, while Sect. 3 is dedicated to the design and development of the setup and nozzle specimens, together with investigated parameters and sensor integration on the test-bench. Section 4 describes a general outline of the test campaign, while Sect. 5 offers a description of the expected results, together with insights on a pre-test for the commissioning of the test-bench. In closure, Sect. 6 summarises the content of the article and gives an outlook on future research activities, including applications beyond the incompressible subsonic counter-flow regimes presented here.



Fig. 1 ANCs models: (**a**) annular aerospike, (**b**) annular-truncated clustered aerospike, (**c**) dual-bell and (**d**) expansion–deflection nozzles. Modified image from Hagemann et al. [8]

(**a**)  (**b**)  (**c**)  (**d**)
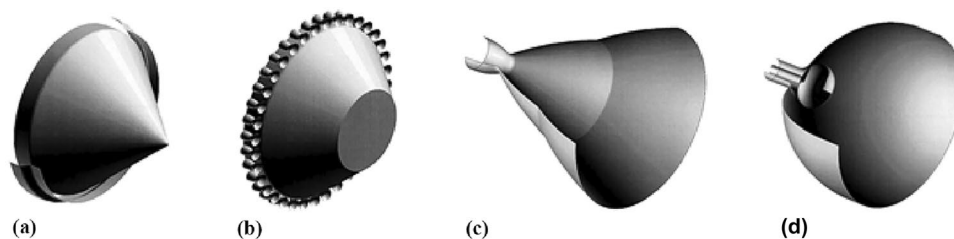
## 2 Methods

The main focus of this investigation is on landing burn manoeuvres [20], during which the reusable main stage experiences a strong variation in counter-flow velocities and ambient-pressure along its trajectory (starting from altitudes of $5 - 10$ km to sea level, from low-supersonic to low-subsonic/motionless). In the framework of testing in the vacuum wind tunnel though, the investigation is limited to a maximum of $\sim 90$ m/s for counter-flow velocities and a minimum of $\sim 7$ kPa for ambient-pressure. This is sufficient to study a wide portion of ambient conditions experienced during the last phase of a landing burn manoeuvre.

The investigation of ANCs described here focuses on annular aerospike, DB and ED nozzles in three distinct ambient conditions, which are defined by:

- near-vacuum ($\sim 7$ kPa) ambient-pressure condition, nozzle cold-flow only;
- SLS (101.325 kPa) ambient-pressure condition, nozzle cold-flow only;
- low-subsonic (up to $\sim 90$ m/s) counter-flows, ambient-pressure conditions from near-vacuum to SLS, with nozzle cold-flow;

The gradual variation of average ambient pressure in the vacuum wind tunnel, from near-vacuum to SLS in a relatively short time (30 sec c.a.), allows the ANCs to exhibit adaptive altitude–compensation. The experimental results on ANCs are then used to compare their performance to a conventional bell nozzle selected as reference model. In particular, the reference bell nozzle shares with the ANCs the same thrust level at their design point.

One way to estimate the losses due to interaction with ambient on the overall performance, is to evaluate them in terms of thrust ($F$) and thrust coefficient ($C_F$), defined, respectively, in Eqs. (1) and (2) [21]:

$$F = C_F \cdot p_c \cdot A_t \tag{1}$$

with $p_c$ as chamber pressure (in isoentropic hypothesis also assumed as $p_{c,0}$, or total chamber pressure) and $A_t$ as nozzle throat area:

$$C_F = C_{F_{opt}} + \frac{A_e}{A_t}\left(\frac{p_e}{p_c} - \frac{p_{amb}}{p_c}\right) \tag{2}$$

with $C_{F_{opt}}$ as optimum thrust coefficient, $p_e$ and $A_e$, respectively, as nozzle exit pressure and exit area and $p_{amb}$ as ambient pressure. In particular, the optimum thrust coefficient is defined as the thrust coefficient corresponding to an optimum expansion ($p_{amb} = p_e$). Indeed, both conventional and advanced nozzles are designed at a specific Nozzle Pressure Ratio ($NPR = p_{c,0}/p_{amb}$), that fully adapts the flow (neither

over-expanded or under-expanded), thus maximising the thrust coefficient for a specific value of ambient pressure ($p_{amb} = p_e$).

In case of optimal expansion, the optimum thrust coefficient defined in Eq. (3) [21], with $\gamma$ as isoentropic exponent, would be the only contribution to the nozzle thrust coefficient in Eq. (2):

$$C_{F_{opt}} = \sqrt{\frac{2\gamma^2}{\gamma - 1}\left(\frac{2}{\gamma + 1}\right)^{(\gamma+1)/(\gamma-1)}\left[1 - \left(\frac{p_e}{p_c}\right)^{(\gamma-1)/\gamma}\right]} \tag{3}$$

while the second contribution to the nozzle performance in Eq. (2), due to pressure differences between ambient and nozzle exit ($p_e$ and $p_{amb}$), would disappear.

For the cold-flow configurations considered, the Aerodynamics Interference (AI) that generates due to the interaction of nozzle flow and counter-flow is described in terms of Mach ($M_\infty$) and Reynolds ($Re_\infty$) numbers for the opposing counter-flow, together with other scaling parameters [6, 22]. In particular, the aerodynamics thrust coefficient ($C_T$), defined in Eq. (4), constitutes a typical parameter to evaluate the magnitude of retro-propulsion on counter-flows:

$$C_T = F/q_\infty A_{ref} \tag{4}$$

where $q_\infty$ is the dynamic pressure of the counter-flow and $A_{ref}$ is a reference area. In this case, $A_{ref}$ corresponds to the cross-sectional area of the cold-flow chamber (for applications on rockets, it is usually the cross-sectional area at the baseplate). It is worth to mention that in this scenario (low-subsonic counter-flow), the aerodynamics thrust coefficient is not as relevant as during a supersonic retro-propulsion for characterising the AI. Nevertheless, the aerodynamics thrust coefficient is evaluated, in accordance to the method adopted by Nonaka et al. [23] for cold-gas thrusters in subsonic counter-flows and in conformity to the aerodynamic database under development (Sect. 4).

Another key parameter for characterising the influence of retro-propulsion on the aerodynamic characteristics is the drag coefficient ($C_D$), defined as

$$C_D = D/q_\infty A_{ref} \tag{5}$$

where $D$ is the force experienced along longitudinal axis in the opposite verse to the counter-flow (i.e., positive if vehicle slows down). $A_{ref}$ is again the cross-sectional area of the cold-flow chamber (coherently with definition of $C_T$ and assuming the model invested by the counter-flow as a blunt-body). According to this definition, in retro-flow operations the thrust increases the drag coefficient (in agreement with Ecker et al. [5]). This is also coherent with the definition of the ballistic coefficient ($\beta = M/C_D A_{ref}$) [1], where $M$ is the total mass of the body and $A_{ref}$ is again the cross-sectional

area at the baseplate. For an RLV during atmospheric re-entry, the ballistic coefficient decreases when experiencing retro-propulsion (higher $C_D$), thus slowing down more efficiently along its trajectory towards landing site. One way to evaluate the contribution to the aerodynamic drag force during active retro-engine phases, is to measure the drag coefficient with only the free-stream being active ($C_{D_{aero}}$), followed by a free-stream combined with an active nozzle flow ($C_{D_{RP}}$). Then, the difference between the two returns the overall increment of drag coefficient ($\Delta C_D$):

$$\Delta C_D = C_{D_{RP}} - C_{D_{aero}} \tag{6}$$

Finally, the increment in drag force is confronted with the thrust level of the nozzle flow in absence of free-stream, to evaluate the variation of aerodynamic drag force due to the jet/free-stream interaction. It gives information on the order of magnitude of the contribution of retro-propulsion to the aerodynamic drag force (expected to drastically decrease as a result of the ejection of the cold-jet [23]).

Such approach gives only a rough estimate of the actual variation of the aerodynamic drag coefficient, as $\Delta C_D$ includes also the effects of the free-stream on the nozzle thrust coefficient. As this latter is expected to be negligible under subsonic counter-flows, the envisaged method constitutes a valid first approach to evaluate the effects of retro-propulsion on the aerodynamic drag coefficient. Nevertheless, it should be clarified that it is not intrinsically true that the retro-propulsion always leads to lower aerodynamic drag coefficients, because the jets directly influence the pressure drag, thus the total drag and the aerodynamic drag cannot formerly be separated. A more precise approach would imply to measure the local static pressure at specific stations on the entire body, then to evaluate the total aerodynamic force contribution along the longitudinal axis. As this solution is not currently implemented on the test-bench, the first approach based on multiple testing has been selected. Nevertheless, the experimental results are backed up by numerical simulations that can derive $C_D$ through the canonical method, thus allowing to evaluate the overall quality of the experimental approach.

## 3 Design and Development of the Test-Bench

In agreement with the above specified methodology, the following section presents the design approach and current state of development of the test-bench for cold-flow tests on ANCs in subsonic counter-flows.
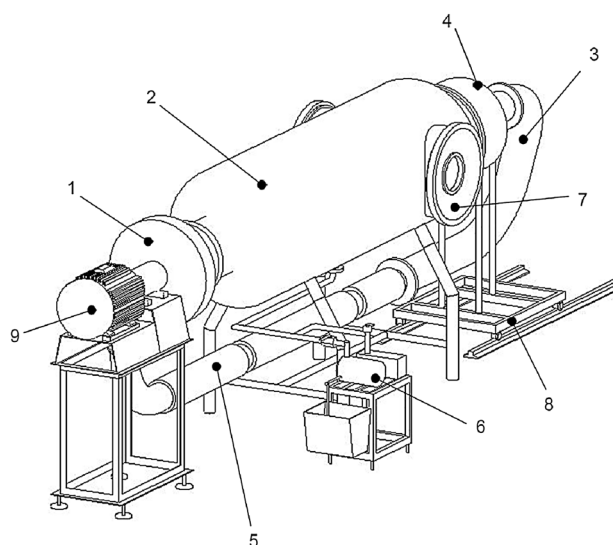
**Fig. 2** Overall schematic of the vacuum wind tunnel: (1) fan, (2) experimental room, (3) ring line, (4) pre-chamber (calming boiler), (5) cooling chambers, (6) evacuation unit, (7) doors with observation window, (8) shifting device of the pre-chamber, (9) drive motor for free-stream generation [24]

### 3.1 Infrastructure and Test-Bench Integration

The cold-gas test-bench is designed for conducting comparative tests on different nozzle models invested by subsonic counter-flows. It is installed into the vacuum wind tunnel at TUD (see Fig. 2). The current infrastructure allows ambient conditions down to near-vacuum ($\sim 7$ kPa), so to realise high pressure ratios between chamber and ambience. As the ambient pressure varies within the chamber, due to the accumulation of gas during any experiment starting from near-vacuum conditions, thus allowing the ANCs exhibit their intrinsic altitude compensation capabilities. The cold-flow fed-system consists of a 350 l tank (gas reservoir in Fig. 3) which provides feeding pressures up to 1.6 MPa for the supplied gas (dry air). The feeding pressure is activated by ball valves and pneumatically controlled via dome-reducers. The fed-line is equipped with a calorimetric flow meter (see Fig. 3). The drive unit (see Fig. 2) dedicated to the free-stream generation is the combination of a fan, a shaft and motor. The radial fan presents a 650 mm diameter, it generates an air-volume flow of 1 m$^3$/s and a maximum pressure ratio of 1.06 (i.e., approx. 6000 Pa pressure difference) at maximum speed ($n = 2940$ rpm) in SLS operative conditions. The pressure ratio is not constant, as it decreases with decreasing absolute pressure in the system, due to the change in the fan flow-pattern. The motor model is an ABB asynchronous motor M2QA180M2A2 (22 kW power), fed by an ABB frequency converter and speed-controlled by in 0.1 Hz steps from $0 - 50$ Hz.

**Fig. 3** Test-bench gas supply and sensor schematic. Modified image from Sieder-Katzmann et al. [18]
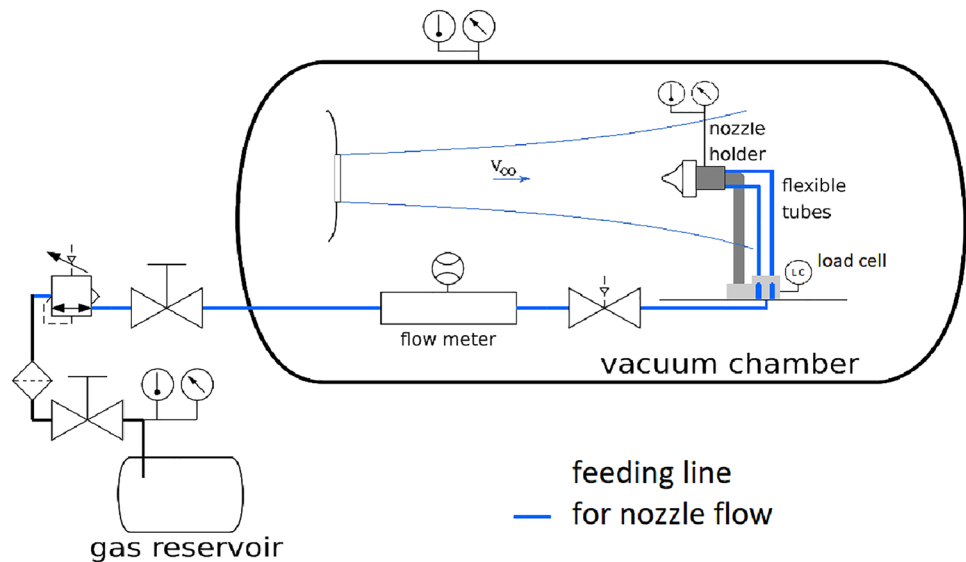


The nozzle holder is positioned longitudinal to the conic flow, as presented in Fig. 3. The free-stream conditions can vary from a minimum Reynolds number of $\sim 7100$ (at $p_{amb} = 10\,\text{kPa}$ and $u_0 = 11\,\text{m/s}$) to a maximum of $\sim 6.53 \times 10^5$ (at $p_{amb} = 101.325\,\text{kPa}$ and $u_0 = 98.7\,\text{m/s}$), where $u_0$ is the axial free-stream velocity at the exit plane of the conical outlet of the chamber. These ambient and free-stream conditions are in agreement with previous studies by Nonaka et al. [23], where the free-stream velocity in the wind tunnel $v_\infty$ is 26.4 m/s and the Reynolds number are approximately $3.5 \times 10^5$ in the critical Reynolds number regime and $5.0 \times 10^6$ in the turbulent-flow regime, respectively. In this case, the counter-flow nozzle diameter is used as the characteristic length for the evaluation of the Reynolds number.

As for Nonaka et al. [23], the Reynolds numbers obtained in the experimental conditions are expected to be lower than those obtained in the real condition by one order of magnitude. Indeed, the free-stream around the model is a transient flow, whereas the flow around the real vehicle is a turbulent flow. In general, these two Reynolds regimes present very different flow-separation points. To verify the independence from Reynolds number of the qualitative fluid-dynamic field around the model invested by a free-stream, a plausible approach would be to verify through optical techniques that the flow separation point is fixed at the corner of the model baseplate, regardless of the Reynolds regime. Once verified, this condition would ensure that the flow-field around the testing model is qualitatively similar to the one around the real vehicle, regardless of the Reynolds number being one order of magnitude lower from that in the real conditions [23]. Therefore, the experimental results would include useful information to qualitatively understand the characterization of the
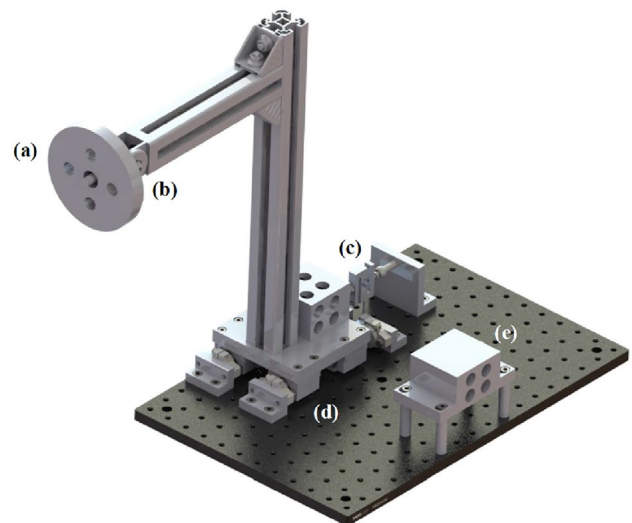


**Fig. 4** CAD model of current test-bench: (**a**) chamber holder, (**b**) adjustable join, (**c**) S-shape load cell, (**d**) sliding system, (**e**) fed-line mounting interface

aerodynamic forces acting on the body in relation to the flow structure due to the free-stream/cold-flow interaction.

The setup is mounted on a bread-board plate (see Fig. 4), so that the test-bench is easily moveable to alternative infrastructures that can realize different retro-flow conditions. The optical bread-board plate mounts:

- sliding support at 1 Degree-Of-Freedom;
- S-shape load cell measuring the horizontal force, connected to the plate by a 90°-angle bracket;
- fed-line mounting interface that connects the setup with the gas supply;

An in-house manufactured base is mounted on top of the sliding system, connected to the shafts by 4 linear bearings. The shafts are connected to standing holders by flanges. The nozzle holder is connected to the test-bench by an "L-shaped" structure of aluminium profiles. The interface between the holder and the profiles is an adjustable join for high loads, up to 100 Nm in the swivel direction, swivel range of 180° and adjustment in the 5° modular dimensions. This solution allows to regulate the Angle-Of-Attack (AOA) easily and ensures a good repeatability of experiments. The flexible tubes of the fed-line are attached directly to the aluminium profiles and go from the mounting interface to the chamber. Their influence in terms of disturbances on the force measurements is taken into account as correctional factors (Sect. 4).

## 3.2 Test Specimens and Cold-Flow Chamber

The current version of the setup might slightly differ from the final outcome, as long as the design and development of the nozzle specimens and cold-gas chamber is still ongoing. Nevertheless, some details are already settled and can be illustrated here.

The cold-flow chamber is designed to host interchangeable nozzle models while keeping the same upstream conditions. The chamber adopts 4 flow inlets and is directly mounted on the adjustable join (Sect. 3.1). In general, NPR and $A_t$ are designed to be equal between the different nozzle specimens, to achieve comparable flow conditions (e.g., thrust level, mass-flow, exit Mach number, total pressure, etc.) at their design point (optimum expansion). This allows to compare the results in off-design ambient conditions, to evaluate the efficiency of the advanced nozzles w.r.t. the conventional bell nozzle. A list of reference values for designing both the nozzle specimens and the cold-flow chamber is shown in Table 1.

The design of the nozzle specimens slightly differs between each model: the contouring for the bell-shaped reference nozzle is a parabolic nozzle contour (based on the Rao parabolic shape [21]), the annular aerospike nozzle contour is derived with an adaption of the FORTRAN code of C. C. Lee. [25], while the DB nozzle design process follows the approach outlined by Génin et al. [26]. A special mention goes to the ED nozzle contour, which is developed in collaboration with "Sapienza" University of Rome and is derived from an adaption of Angelino's method [27]. The nozzle specimens are manufactured with

**Table 1** Preliminary design parameters for nozzle specimens and flow chamber

| Parameter | Symbol | Value | Unit |
|---|---|---|---|
| Nozzle pressure ratio | $NPR_{o.d.}$ | 45 | – |
| Chamber total pressure[1] | $p_{c,0}$ | 0.48 | MPa |
| Chamber total temperature | $T_0$ | 293.15 | K |
| Chamber cross-sectional area | $A_c$ | 5541.8 | mm$^2$ |
| Isoentropic exponent | $\gamma$ | 1.4 | – |
| Specific gas constant (air) | $R$ | 287 | J/kg K |
| Nozzle expansion ratio[2] | $\varepsilon$ | 4.82 | – |
| Nozzle throat area | $A_t$ | 58.5 | mm$^2$ |
| Mass-flow[3] | $\dot{m}$ | 80.0 | g/s |
| Thrust[3] | $F$ | 40.0 | N |

1 Assumed $NPR \approx p_1/p_{amb}$, as $p_1 \approx p_{c,0}$ (valid for a nozzle entrance ratio: $A_1/A_t \geq 4$ [21]), where $p_1$ is the static pressure at the nozzle inlet.
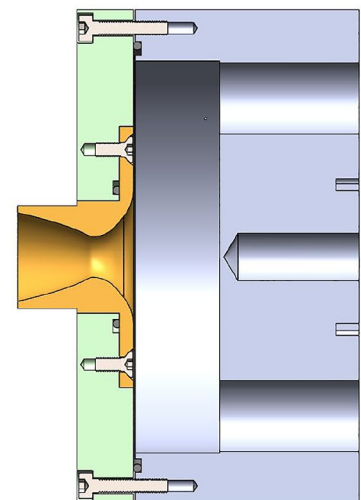
2 By definition: $\varepsilon = A_e/A_t$.

3 Expected values, in hypothesis of isoentropic nozzle flow



**Fig. 5** CAD model, example of the final setup, in a configuration mounting a conventional bell nozzle: front (**a**) and side (**b**) views of the cold-flow chamber. Respectively, the chamber base (in *grey*), the front-plate (in *green*) and the nozzle specimen (in *yellow*)
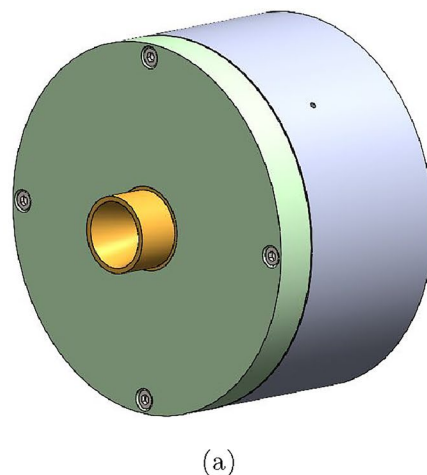
(a)

(b)

a stereolithographic additive layer manufacturing (ALM) process, using the printer model Form 2 by Formlabs®.

The setup presents a dis-mountable front-plate (see Fig. 5, in *green*), that allows the nozzle specimens (in *yellow*) to be inter-changeable. This design approach ensures a relatively high replicability of the chamber conditions between the different test cases, thus enhancing the quality of results coming from any comparative analysis to follow. The adoption of annular aerospike and ED nozzles, due to the presence of an internal body (i.e., spike and pintle for aerospike and ED nozzle, respectively), might imply minor changes at design level on the front-plate, while leaving the chamber base (see Fig. 5, in *grey*) unchanged between the different test cases.

The actual performance could slightly differ from the values predicted at the nozzles design point due to manufacturing imperfection ($25 - 100\,\mu m$ limit in ALM printing resolution, depending on resin choice) [28]. The nozzle model mounted during the commissioning pre-test (see Sect. 5) was additively manufactured with a Tough 1500 resin, that was used as material for the first version. In future, the models will be printed with a Dental Model resin, as a peculiar combination of printer and material has been found to be the best compromise. Indeed, it provides a hydraulically smooth surface and ensures a dimensionally accurate reproduction of the CAD model under most of circumstances [29].

Other sources of error are disturbance forces due to the flexible tubing (they can only be eliminated to a certain extent, see Sect. 4) and discrepancies on assumptions and boundary conditions w.r.t. the one-dimensional models used as reference for design [18]. On the other hand, the pressure losses along the feeding system can be assumed as negligible if the set chamber pressure ($p_c$) is fully achieved during the experiments. It is due to notice that there is no strict requirement on a specific thrust value to satisfy. The mandatory result though, is that these values are comparable between all the different nozzles at their design point ($NPR_{o.d.} = 45$).

## 3.3 Data Acquisition System, Sensors and Visualisation

The sensors involved lie within four main types: force sensors, pressure sensors, thermocouples and mass-flow sensors. The force sensor is an S-shape load cell, model KD40s 100N/XP001 from ME-Meßsysteme GmbH®. It is a special version, suitable for vacuum ($p < 10^{-5}$ mbar). The nominal force is 100 N in an accuracy class of 0.1 %. It comes with a 5p/m/M12/TEDS connector, including the transducer electronic data sheet (TEDS) and is interfaced to a GSV-6K, a signal conditioner which provides an industrial standard sensor signal. In particular, the TEDS functionality allows to compensate the sensor characteristic and work with a nominal measurement signal for force value conversion. This is especially useful in case of exchanging the force sensor [18].

The pressure measurements in the cold-flow chamber require a high accuracy absolute measuring sensor, an S-20 type with range $0 - 1$ MPa (abs) and accuracy $\pm 0.125\%$ (of full-range). Instead, for measuring tank pressure and pilot pressures for the dome-regulators, standard type A-10 industrial gauge pressure sensors are used, with, respectively, ranges of $0 - 1.6$ MPa (abs) for the tank and $0 - 1$ MPa (abs) for the pilot pressures, and a common accuracy of $\pm 0.5\%$ (of full-range). All the pressure sensors are provided by WIKA Alexander Wiegand SE & Co. KG® [18]. Thermocouples type K are used in cold-flow chamber and supply tank. They are manufactured by THERMA Thermofühler GmbH and specified to be compliant to the German standard DIN IEC 60584-3 with an accuracy of $\pm 1.5$ K [18].

The mass-flow on the feed-line is measured with calorimetric sensors type VA 520 F from CS Instruments®, measurement range of $0 - 240.0$ g/s ($670$ Nm³/h). A five-point manufacturer calibration is used, which reduces the measurement error to $\pm 1$ % of the measurement value or $\pm 0.3$ % full scale range [18].

The Data Acquisition System (DAQ-System) is a NI cDAQ-9189 from National Instruments®, interfaced with a dedicated LabVIEW® routine. The latter will include specific functionalities that automatise calibration procedures (e.g., thrust correction due to parasite forces on tubing), monitor specific warning parameters, implement automatic

**Table 2** List of input modules currently mounted on cDAQ-9189 in the vacuum wind tunnel facility (TUD)

| Qnt. | Model | Typology | Channels | Update rate[1] | Resolution |
|---|---|---|---|---|---|
| 1 | NI-9213 | Thermocouples | 16 | 75 S/s | 24 bits ADC |
| 2 | NI-9203 | Input analog current[2] | 8 | 200 kS/s | 16 bits ADC |
| 1 | NI-9265 | Output analog current[3] | 4 | 100 kS/s | 16 bits DAC |
| 1 | NI-9474 | Digital output | 8 | 1 µs | – |

1 Max sample-rate for analog I/O cards (Sample/s) *or* max delay-time for digital outputs cards only (µs).

2 Input current: $\pm 20$ mA.

3 Output current: $0 - 20$ mA

shut-down procedures for safety in case of malfunction and communicate results directly to the database for ANCs in different retro-engine operations. The I/O-Modules control the test-bench and read the analogue sensor data. The control outputs act on the solenoid valves (which control the ball valves) and on the electric pressure regulators (which act on the dome-regulators) [18]. Currently, five module slots are used on the cDAQ-9189. A list of the mounted cards is given in Table 2. In addition to these, the digital I/O module NI-9402 module will be mounted for BOS triggering.

For flow visualisation, a Background-Oriented Schlieren (BOS) system is adopted. The optical access on the area of interest is realised in correspondence of the nozzle exit section with opposing glass windows in the vacuum chamber [18]. A high speed Flir Blackfly S Camera (model BFS-U3-51S5M-C) in combination with a Tokina machine vision lens (model TC2514-10MP) has been selected. To improve the contrast, the lens mounts a green bandpass filter (BP525-37.5) by MidOpt, while the background is illuminated with green monochromatic light. The choice of a BOS, instead of a classic Z-type schlieren system, is encouraged by relatively lower efforts for the installation of the optical system, together with satisfying results on past experimental campaigns that returned qualitative visualisation on the flow-field [18]. Eventually, this comes with a lower spatial resolution and a limited real-time imaging (i.e., post-processing is always needed for BOS) [30] w.r.t. any Z-type schlieren system.

## 4 Test Campaign Outline

The methodology introduced in Sect. 2, together with the solutions adopted in Sect. 3, contribute to define a foreseeable outline for the conduction of future test sessions on ANCs in the vacuum wind tunnel. The experimental campaign will be structured in multiple tests on various nozzle models (Sects. 2 and 3) for a span of counter-flows and ambient conditions, with the final purpose of conducting a comparative study on conventional nozzles and ANCs. To each category of test cases (see Table 3) corresponds a

**Table 3** List of test cases (common between the different nozzle specimens) for the experimental campaign

| Parameter | Unit | Case 1 | Case 2 | Case 3 | Case 4[1] |
|---|---|---|---|---|---|
| $p_{c,0}$ | MPa | 0.480 | 0.480 | 0.101 | 0.480 |
| $u_0$ | m/s | 0.00 | 0.00 | 90.00 | 90.00 |
| $p_{amb}$ | kPa | 10.000 | 101.325 | 101.325 | 101.325 |
| $Re_\infty$ | – | 0.0 | 0.0 | $\sim 595\,400$ | $\sim 595\,400$ |

1 The test case will be repeated for values of AOA that span from 0.0°. to 20.0° in steps of 5.0°

specific investigation: test cases that do not involve counter-flows (Cases 1–2) are dedicated to verify the expected thrust level for each nozzle model, at their design point and specific off-design points; the test case with subsonic counter-flow but without nozzle flow (Case 3) delivers the evaluation of aerodynamic drag force and coefficient; the retro-flow test (Case 4), that combines nozzle-flow and counter-flow, determines the aerodynamics thrust coefficient, the impact of retro-propulsion on the aerodynamic drag coefficient (depending on AOA) and the achievable thrust gains for ANCs under different counter-flows.

In addition to these, further investigations will follow on adaptive altitude compensation with variable ambient pressure from near-vacuum to SLS conditions. It is due to mention that, within the test campaign, the investigation of some complex phenomena related to ANCs will be neglected for simplicity of first analysis; this includes additional side-loads during transient phases or transition between different operative modes (e.g., from sea-level mode to altitude-mode for DB nozzle, from open-wake to closed-wake for aerospike and ED nozzle [8]).

The experimental results are compared with numerical results adopted in the design phase (in quasi-one-dimensional nozzle flow hypothesis) and with CFD simulations in AnSYS Fluent®, to validate the latter. Once the reliablilty of the experimental results is validated (i.e., in case of non-zero AOA, repetition of test at corresponding negative AOA is due) and the data evaluation is performed, all the results will be archived in a dedicated aerodynamic database. The latter will contain ANCs in different retro-flow conditions, together with the counter-flow conditions (i.e., $M_\infty$ and $Re_\infty$) and scaling parameters (e.g., $C_T$) associated to each specific test case.

To derive the characteristic $M_\infty$ and $Re_\infty$, it would be necessary to determine the velocity profiles of the counter-flow within the test chamber. This is achieved through dedicated test campaigns involving measurements with Pitot tubes or hot-wire anemometers. A similar approach has been adopted in the past during the re-commissioning test campaign of the vacuum wind tunnel facility. The technical reports recorded the velocity profiles of the free-stream at different chamber pressures and flow velocities. An example of velocity profiles, as recorded in these internal reports, is presented in Fig. 6. The quantities here involved are: longitudinal distance between the chamber base-plate and the free-stream outlet ($x$), referred to the diameter of this latter ($d = 100$ mm); vertical distance from the free-stream axis of symmetry ($y$), referred to the outlet radius ($r = 50$ mm); axial air speed at the $x$ station ($u_x$), referred to the axial exit velocity at the free-stream outlet ($u_0 = 90$ m/s); ambient pressure inside the test chamber ($p = 101.325$ kPa).

In incompressible flow hypothesis ($M_\infty < 0.3$) [31], it is assumed Bernoulli's principle to be valid and one can derive

**Fig. 6** Example of velocity profiles, derived during the commissioning tests of the vacuum wind tunnel in TUD [24]
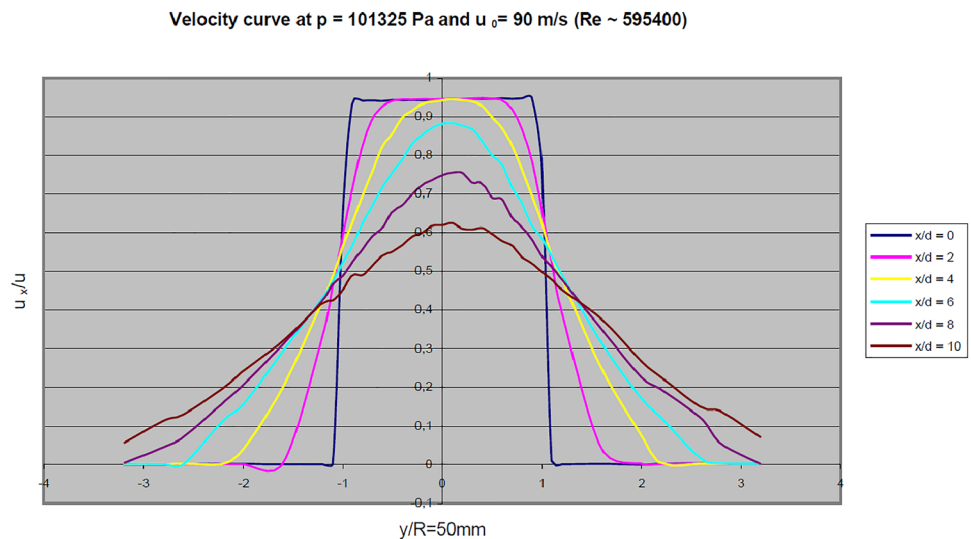
velocities by comparing the dynamic pressure of the counter-flow ($q_\infty = 1/2\rho_\infty v_\infty^2$) with the total pressure ($p_{\infty,0}$). It is also due to evaluate the local velocity of sound, by deriving it from static temperature measurements ($a_\infty = \sqrt{\gamma R T_\infty}$). This allows to calculate the aerodynamic (theoretical) coefficient based on the measurement of the velocity profile of the free-stream. In real case though, the presence of Pitot tubes inevitably alters the aerodynamic field around the body, thus supporting the adoption of a different strategy. One envisaged solution is to verify experimentally the velocity profiles and confront them with the ones tabled in the internal reports for calibration of the free-stream conditions. Once the velocity profiles are verified, they would be assumed as valid during the experiments for the derivation of the aerodynamic coefficients. Then, a second verification step would follow by the end of the test campaign.

The conical subsonic free-stream presents different velocity profiles depending on the distance from the exit plane of the test-chamber outlet ($x/d$). This is a free parameter that needs to be tuned, to find a compromise between a relatively uniform velocity profile investing the set-up and the disturbances on the free-stream, generated by the nozzle flow, that could go upstream into the pre-chamber (see Fig. 2). This value of $x/d$ is chosen to be between 1 and 2, where x is the longitudinal distance between the chamber base-plate and the wind tunnel outlet and d is the diameter of the outlet ($d = 100$ mm). Due to the strong contraction of the air-flow between the pre-chamber and the outlet of the vacuum wind tunnel (from 800 mm diameter to 100 mm) there is a significant pressure loss; this is expressed in a $(u_x/u_0)_{max}$ ratio of about 0.9–0.96 (see Fig. 6).

Before the actual campaign starts, preliminary tests are required, to correct measurement errors due to the forces generated by the pressure within the flexible gas-supply tubes. For that reason, a data set based on force measurements with closed gas outlets is acquired for the complete pressure range: the measured disturbance forces are then modelled through a quadratic polynomial with the pressure differences acting on the tubes ($\Delta p$), which is then adopted to correct the force measurements by subtraction.
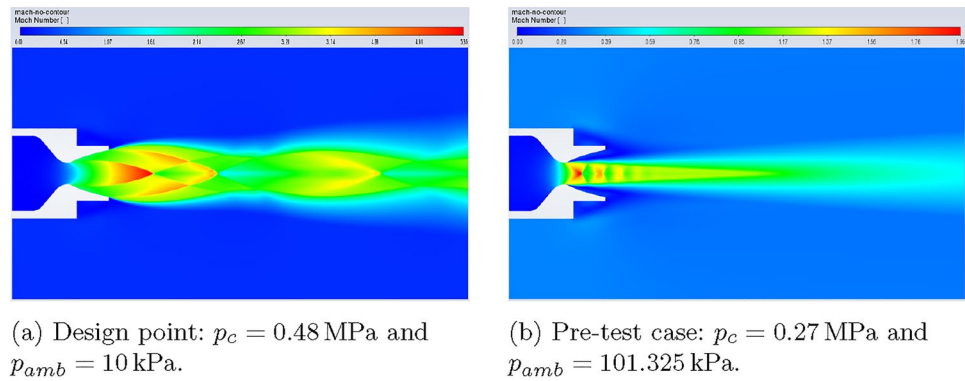
In closure, an additional test campaign is dedicated to ED nozzles, based on comparative tests between different geometrical properties (i.e., aspect-ratio and volumetric encumbrance), exclusively in near-vacuum ambient conditions. In this regard, a clarifying example could be the investigation on reduction of volumetric encumbrance that an ED solution realises w.r.t. a conventional bell nozzle (for same thrust level and specific impulse on design at near-vacuum ambient conditions).

## 5 Commissioning Pre-test, Expected Results and Discussion

First preliminary results come from the commissioning pre-test carried out for the commissioning of the test-bench. The latter was carried out mainly to verify the correct installation of the setup in the vacuum wind tunnel facility. As nozzle specimen, a standard parabolic bell nozzle has been selected (Sect. 3). Such a nozzle is designed for near vacuum conditions and, differently from ANCs, experiences high overexpansion at SLS conditions. This behaviour is visible in Fig. 7b, which clearly presents flow separation at nozzle wall for $p_c = 0.27$ MPa (in agreement with Summerfield criterion [32]).

While the measurements acquired during the commissioning pre-test for pressure, temperature and mass-flow are delivered by calibrated sensors, the force levels (see Fig. 8) are not yet corrected for the parasite forces generated by the flexible tubing (Sect. 4). At $p_c = 0.27$ MPa (56

**Fig. 7** CFD simulations: Mach number for Rao parabolic nozzle in various ambient conditions. Chamber conditions are: $T_c = 280.0$ K, $p_c = 0.48$ MPa (**a**) and $p_c = 0.27$ MPa (**b**)



(a) Design point: $p_c = 0.48$ MPa and $p_{amb} = 10$ kPa.

(b) Pre-test case: $p_c = 0.27$ MPa and $p_{amb} = 101.325$ kPa.

**Fig. 8** Results from commissioning pre-test, in order (left–right, top–down): chamber pressure (Pa), chamber temperature (°C), primary mass-flow (kg/s) and nominal thrust (N)
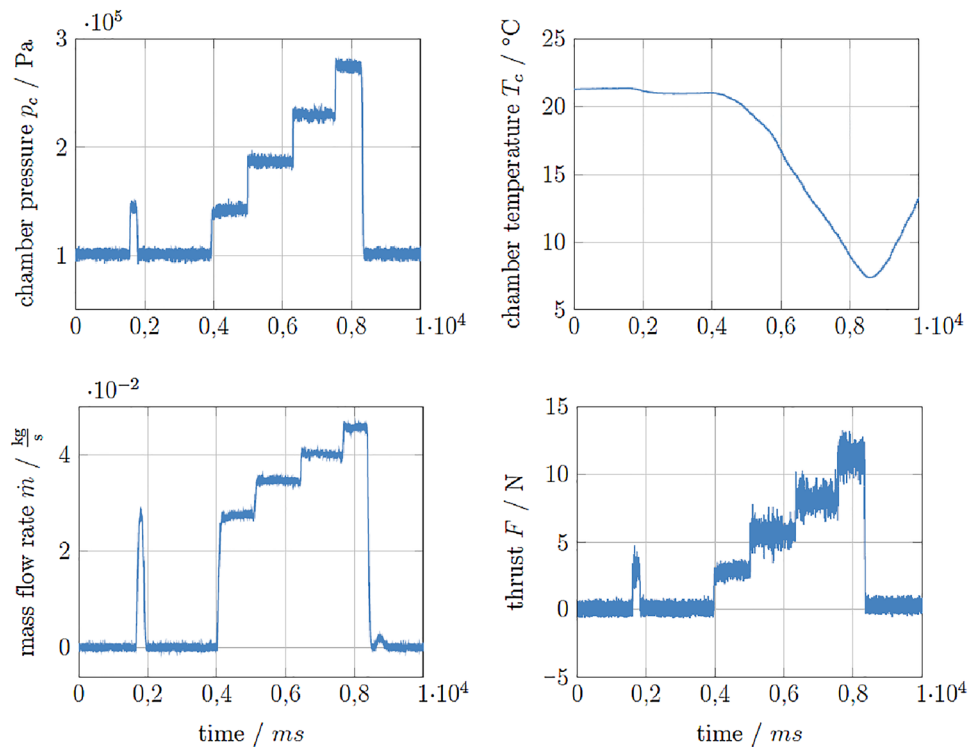


% of chamber pressure on design, see Table 1), results in a relative error on the thrust level of around 4 % (13.4 N against 12.9 N, respectively), by confronting experimental and numerical axial force. Such a 0.5 N difference can be explained with several reasons: lack of CFD models validation, as this will be addressed in parallel with the actual test campaign; surface roughness, as a limited printing resolution of the ALM process (Sect. 3.2) determines additional pressure losses; absence of preliminary force sensor calibration also has an impact on results. Further investigations on thrust losses will be addressed during the experimental campaign. Nevertheless, it is important to stress that neither the experimental nor CFD results should be addressed as realistic before carrying out some preliminary operations: the parasite forces calibration needs to be conducted, then the force sensor off-set value needs to

be verified with a precision tool (as a professional spring balance). Eventually, this value can be assumed as correct and then used as validation data for the CFD models.

Another phenomenon that requires attention is the gradual decrease in chamber temperature ($\Delta T_c \approx 14$ °C) during the experiment: such a rapid change is an unavoidable consequence of the expansion of dry-air. A foreseeable solution to achieve the expected design conditions in the cold-flow chamber (Sect. 3.2) would be to pre-heat the gas and collect data in correspondence of the design point, while chamber temperature is dropping. Such approach would result beneficial also to avoid the phenomenon of condensation [22, 33], whose influence could manifest during the comparison of experiments and computations (where condensation is neglected). Further insights on

feasible heating solutions to implement on the test-bench will be addressed during research activities to follow.

The BOS post-processing, executed on several frames captured during the commissioning pre-test, returned mediocre qualitative results due to hardware limitations and a relatively low image exposure. The first issue will be solved by inserting the camera directly inside the test chamber, while the latter can be enhanced by properly tuning aperture and exposure time, thus reducing the ISO-levels (i.e., increasing the signal-to-noise index).

The reference results coming from literature review on conventional bell nozzles in retro-engine operations [4–7, 22, 23], together with preliminary results from the commissioning pre-test, outline the expected outcome of the test campaign on ANCs to follow. The impact of the retro-propulsion on the actual performance and altitude–compensation efficiency of the nozzle should be minimum, due to the low-subsonic counter-flows speed, while the impact on the aerodynamic drag would be more evident. Indeed, the aerodynamic drag is expected to decrease in one order of magnitude, in presence of subsonic counter-flows comparable with the ones considered by Nonaka et al. [23]. Moreover, this decrement should become larger by increasing the aerodynamics thrust coefficient, with a higher dependency on $C_T$ for values of it between 0.0 and 0.2 [23]. Similarly, such a phenomenon is experienced also by involving supersonic counter-flows [5, 6, 22], resulting in some cases in a negligible or even negative aerodynamic drag coefficient. Under subsonic counter-flow conditions, the reduction of pressure drag at the base-plate surface is mainly caused by the blockage of the free-stream by nozzle jet and flow recirculation areas. On contrary, the surface pressure on all sides beyond the base-plate is expect to increase, thus confirming the influence of the nozzle jet on the flow-field beyond the model side. The overall effect of the jet/free-stream interaction would be a reduced drag force acting on the model, in accordance to Nonaka et al. [23]: the recirculation area formed by the jet/free-stream interaction causes a decrease in the surface pressure on the base-plate; this mechanism suppresses the flow separation at the corner of the base-plate and causes an increase in pressure on the side and back surfaces. As a consequence of the cold-flow jets pushing against the free-stream, the aerodynamic drag force acting on the model decreases. On contrary, a different behaviour is experienced by the overall drag force, which generally increases thanks to the contribution of the active retro-engine (Sect. 2).

## 6 Conclusions and Outlook

A general overview on the test-bench for cold-flow testing of ANCs in subsonic counter-flow has been presented. It goes through the design of cold-flow chamber and test specimens, the configuration and installation of the setup in the vacuum wind tunnel, as well as the DAQ systems, the integration of sensors and visualisation technique adopted. An outline of the future test campaign describes the investigation scenarios, common to each nozzle type and distinct by free-stream and ambient conditions. The expected results on thrust level and aerodynamics thrust coefficient foresee a small impact of counter-flows on the retro-propulsion, mostly dominated by the nozzle cold-flow. Nevertheless, the impact of the active cold-flows on aerodynamic drag is expected to be more evident, as the jet/free-stream interaction strongly re-shapes the flow-field around the model. Moreover, the method of analysis could be extended to further cases of interest, such as compressible counter-flow regimes at free-stream Mach values higher than 0.3. In this regard, the design and portability of the test-bench envisages its integration in infrastructures with compressible subsonic counter-flows capabilities.

The commissioning pre-test was addressed as successful, as it proved the full compatibility of the setup with the vacuum wind tunnel infrastructure. Moreover, it returned useful inputs for improving the overall quality of results from the following-up test campaign on ANCs. Further corrections are needed on the thrust levels, due to generation of parasite forces by the flexible tubing, as well as further improvements on the exposure settings for BOS.

The cold-flow testing on ANCs in retro-flow configuration foreseen in future activities is not limited to extensions of this specific test campaign. Indeed, the delivered methodology and results define the first guidelines for the future activities by the research group on both supersonic and compressible subsonic counter-flow regimes. Moreover, they contribute to validate the CFD models in AnSYS Fluent©, currently under development in TUD. In particular, these models could be extended to additional cases out of range for the experimental campaigns and so contributing to enrich the aerodynamic database on ANCs in different retro-flow scenarios. In conclusion, the foreseeable activities, both experimental and numerical, aim to understand the behaviour of ANCs in retro-flow scenarios and, eventually, investigate them as alternative solutions to bell nozzles for reusable main stages.

## Declarations

**Author contributions** Dipl.-Ing. JS-K co-supervises students' projects (directly involved in the test campaign) and reviewed this article.

Dr.-Ing- CB supervises the individual research program of the main author and reviewed the article. Dipl.-Ing. F W designed the ED nozzle contour and collaborated in defining the dedicated test campaign. Mr. FR designed and developed the test-bench and the CAD models in the framework of his student project. Mr. CTM contributed to this paper with CFD simulations and by designing the Rao nozzle contour. All the other co-authors were involved in the review process in role of academic supervisors and approved the publication of this article.

## References

1. Stappert, S., Wilken, J., Bussler, L., Sippel, M.: A systematic assessment and comparison of reusable first stage return options. In: 70th International Astronautical Congress (IAC), Washington, D.C., USA (2019). https://elib.dlr.de/133400/

2. Vernacchia, M.T., Mathesius, K.J.: Strategies for reuse of launch vehicle first stages. In: 69th International Astronautical Congress 2018, Bremen, DE (2018). IAC-18-D2.4.3. https://github.com/mvernacc/lvreuse/blob/master/paper/IAC-18-D-2-4-3_strategies_for_reuse_of_launch_vehicle_first_stages.pdf

3. Dumont, E., Ecker, T., Chavagnac, C., Witte, L., Windelberg, J., Klevanski, J., Giagkozoglou, S.: Callisto - reusable vtvl launcher first stage demonstrator. In: 6th Conference on Space Propulsion, Sevilla, ES (2018). https://elib.dlr.de/119728/1/406_DUMONT.pdf

4. Marwege, A., Gülhan, A., Klevanski, J., Riehmer, J., Kirchheck, D., Karl, S., Bonetti, D., Vos, J., Jevons, M., Krammer, A., Carvalho, J.: Retro propulsion assisted landing technologies (retalt): Current status and outlook of the eu funded project on reusable launch vehicles. In: 70th International Astronautical Congress (IAC), Washington, D.C., USA (2019). https://www.retalt.eu/cloud/index.php/s/jng5JzdGLTmZ74a

5. Ecker, T., Zilker, F., Dumont, E., Karl, S., Hannemann, K.: Aerothermal analysis of reusable launcher systems during retro-propulsion reentry and landing. In: 6th Conference on Space Propulsion. American Institute of Aeronautics and Astronautics, Sevilla, ES (2018). https://elib.dlr.de/120072/1/00040_ECKER.pdf

6. Korzun, A.M., Cassel, L.A.: Scaling and similitude in single nozzle supersonic retropropulsion aerodynamics interference. In: AIAA Scitech 2020 Forum. American Institute of Aeronautics and Astronautics, Orlando, FL, USA (2020). https://doi.org/10.2514/6.2020-0039

7. Stappert, S., Sippel, M.: Critical analysis of spacex falcon 9 v1.2 launcher and missions. Technical report, DLR (November 2017). https://elib.dlr.de/120183/

8. Hagemann, G., Immich, H., Nguyen, T.V., Dumnov, G.E.: Advanced rocket nozzles. J. Propulsion Power **14**(5) (1998). https://doi.org/10.2514/2.5354

9. Onofri, M., Calabro, M., Hagemann, G., Immich, H., Sacher, P., Nasuti, F., Reijasse, P.: Plug nozzles: summary of flow features and engine performance - overview of RTO/AVT WG 10 subgroup 1. In: 40th AIAA Aerospace Sciences Meeting & Exhibit. American Institute of Aeronautics and Astronautics, Reno, NV, USA (2002). https://doi.org/10.2514/6.2002-584. https://arc.aiaa.org/doi/10.2514/6.2002-584

10. Bach, C., Schöngarth, S., Bust, B., Propst, M., Sieder-Katzmann, J., Tajmar, M.: How to steer an aerospike. In: 69th International Astronautical Congress (IAC), Bremen, Germany (2018). https://www.researchgate.net/publication/328145907_How_to_steer_an_aerospike

11. Taylor, N.V.: Simulating cross altitude performance of expansion deflection nozzles. In: 57th International Astronautical Congress, vol. 14, 5, pp. 620–634. American Institute of Aeronautics and Astronautics, Valencia, SP (2006). https://doi.org/10.2514/6.iac-06-c4.5.07

12. Bolgar, I., Scharnowski, S., Kähler, C.J.: Transition of a dual-bell nozzle with an external flow transonic vs. supersonic transition. In: DFG SFB TRR40 Annual Report 2018, pp. 135–146. Deutsche Forschungsgemeinschaft, (2019). https://doi.org/10.13140/RG.2.2.33505.53606

13. Bolgar, I., Scharnowski, S., Kähler, C.J.: Experimental analysis of the interaction between a dual-bell nozzle with an external flow field aft of a backward-facing step. New Results in Numerical and Experimental Fluid Mechanics XII, 405–415 (2019). https://doi.org/10.1007/978-3-030-25253-3_39

14. Bach, C., Schmiel, T., Propst, M., Sieder-Katzmann, J., Tajmar, M.: Key Technologies for Space Exploration developed at TU Dresden. In: Global Space Exploration Conference (GLEX 2021), St. Petersburg, RS (2021). https://iafastro.directory/iac/paper/id/63051/summary/

15. Sieder-Katzmann, J., Propst, M., Stark, R., Schneider, D., General, S., Tajmar, M., Bach, C.: ACTiVE - Experimental set up and first results of cold gas measurements for linear aerospike nozzles with secondary fluid injection for thrust vectoring. In: 8TH EUROPEAN CONFERENCE FOR AERONAUTICS AND AEROSPACE SCIENCES (EUCASS). Proceedings of the 8th European Conference for Aeronautics and Space Sciences, Madrid, SP (2019). https://doi.org/10.13009/EUCASS2019-465

16. Buchholz, M., Gloder, A., Gruber, S., Marquardt, A., Meier, L., Müller, M., Propst, M., Riede, M., Selbmann, A., Sieder-Katzmann, J., Tajmar, M., Bach, C.: Developing a roadmap for the post-processing of additively manufactured aerospike engines. In: 71st International Astronautical Congress (IAC) (2020). https://www.researchgate.net/publication/356634434_Developing_a_roadmap_for_the_post-processing_of_additively_manufactured_aerospike_engines

17. Propst, M., Sieder-Katzmann, J., Stark, R., Schneider, D., General, S., Tajmar, M., Bach, C.: Active - optimisation of a fluidic thrust vector control on aerospike nozzles. In: Space Propulsion Conference (2021)

18. Sieder-Katzmann, J., Propst, M., Tajmar, M., Bach, C.: Investigation of aerodynamic thrust-vector control for aero-spike nozzles in cold-gas experiments. In: Space Propulsion Conference (2021). https://www.researchgate.net/publication/350849794_INVESTIGATION_OF_AERODYNAMIC_THRUST-VECTOR_CONTROL_FOR_AERO-_SPIKE_NOZZLES_IN_COLD-GAS_EXPERIMENTS

19. Taylor, N.V., Hempsell, C.M., Macfarlane, J., Osborne, R., Varvill, R., Bond, A., Feast, S.: Experimental investigation of the

evacuation effect in expansion deflection nozzles. Acta Astronautica **66**, 550–562 (2010). https://doi.org/10.1016/j.actaastro.2009.07.016

20. Kirchheck, D., Marwege, A., Klevanski, J., Riehmer, J., Gülhan, A.: Validation of wind tunnel test and cfd techniques for retropropulsion (RETPRO): Overview on a project within the future launchers preparatory programme (flpp). In: Conference: International Conference on Flight Vehicles, Aerothermodynamics and Re-entry Missions & Engineering (FAR), Monopoli, Italy (2019)

21. Sutton, G.P., Biblarz, O.: Ch. 3, "Nozzle Theory and Thermodynamic Relations". ROCKET PROPULSION ELEMENTS, Ed. 9 edn., pp. 5062–6372. WILEY, Wiley, Hoboken, NJ, USA (2016). https://www.ebook.de/de/product/23826026/george_p_sutton_oscar_biblarz_rocket_propulsion_elements_9_e.html

22. Gutsche, K., Marwege, A., Gülhan, A.: Similarity and key parameters of retropropulsion assisted deceleration in hypersonic wind tunnels. J. Spacecraft Rockets **58**(4), 984–996 (2021). https://doi.org/10.2514/1.a34910

23. Nonaka, S., Nishida, H., Kato, H., Ogawa, H., Inatani, Y.: Vertical landing aerodynamics of reusable rocket vehicle. Trans. Jpn. Soc. Aeronaut. Space Sci Aerospace Technol. Jpn. **10**, 1–4 (2012). https://doi.org/10.2322/tastj.10.1

24. Leonhardsberger, M., Strohmer, P.: Erprobung und dokumentation eines windkanals für verdünnte gase. ILR-NWK G 04-10 (TUD Report) (2004)

25. Lee, C.C.: Technical note— fortran programs for plug nozzle design. Technical report, Scientific Research Laboratories, Brown Engineering Company, Inc. (March 1963). Scientific Research Laboratories, Brown Engineering Company, Inc. https://archive.org/details/nasa_techdoc_19630012259/page/n9/mode/2up

26. Génin, C., Stark, R., Quering, K., Frey, M., Ciezki, H., Haidn, O.: Dual bell nozzle contour optimization. In: Sonderforschungsbereich/Transregio 40 - Annual Report 2012. Springer, (2012). https://elib.dlr.de/92258/

27. Angelino, G.: Approximate method for plug nozzle design. AIAA J. **2**(10), 1834–1835 (1964). https://doi.org/10.2514/3.2682

28. Formlabs: Form 2 3D Printer, Tech Specs. Formlabs official site. (accessed on 28.01.2022) (2022). https://formlabs.com/3d-printers/form-2/tech-specs/

29. Sieder-Katzmann, J., Propst, M., Tajmar, M., Bach, C.: Cold gas experiments on linear, thrust-vectored aerospike nozzles through secondary injection. In: 70th International Astronautical Congress (IAC), Washington D.C., United States (2019)

30. Settles, G.S., Hargather, M.J.: A review of recent developments in schlieren and shadowgraph techniques. Measurement Science and Technology **28**(4) (2017). https://doi.org/10.1088/1361-6501/aa5748

31. Anderson, J.: Modern Compressible Flow : with Historical Perspective. McGraw-Hill, Boston (2003). https://www.mheducation.com/highered/product/modern-compressible-flow-historical-perspective-anderson/M9781260471441.html

32. Stark, R.: Flow separation in rocket nozzles, a simple criteria. In: 41st AIAA/ASME/SAE/ASEE Joint Propulsion Conference & Exhibit. American Institute of Aeronautics and Astronautics, Tucson, Arizona, USA (2005). https://doi.org/10.2514/6.2005-3940

33. Wegener, P.P., Mack, L.M.: Condensation in supersonic and hypersonic wind tunnels. In: Advances in Applied Mechanics, pp. 307–447. Elsevier, Jet Propulsion Laboratory. California Institute of Technology. Pasadena. California, USA. (1958). https://doi.org/10.1016/s0065-2156(08)70022-x